

RSGPT: A Remote Sensing Vision Language Model and Benchmark

Yuan Hu[†], Jianlong Yuan[†], Congcong Wen, *IEEE Member*, Xiaonan Lu, Xiang Li*, *IEEE Member*.

Abstract—The emergence of large-scale Large Language Models (LLMs), with GPT-4 as a prominent example, has significantly propelled the rapid advancement of Artificial General Intelligence (AGI) and sparked the revolution of Artificial Intelligence 2.0. In the realm of remote sensing, there is a growing interest in developing large vision language models (VLMs) specifically tailored for data analysis in this domain. However, current research predominantly revolves around visual recognition tasks, lacking comprehensive, large-scale image-text datasets that are aligned and suitable for training large VLMs, which poses significant challenges to effectively training such models for remote sensing applications. In computer vision, recent research has demonstrated that fine-tuning large vision language models on small-scale, high-quality datasets can yield impressive performance in visual and language understanding. These results are comparable to state-of-the-art VLMs trained from scratch on massive amounts of data, such as GPT-4. Inspired by this captivating idea, in this work, we build a high-quality Remote Sensing Image Captioning dataset (RSICap) that facilitates the development of large VLMs in the remote sensing field. Unlike previous remote sensing datasets that either employ model-generated captions or short descriptions, RSICap comprises 2,585 human-annotated captions with rich and high-quality information. This dataset offers detailed descriptions for each image, encompassing scene descriptions (e.g., residential area, airport, or farmland) as well as object information (e.g., color, shape, quantity, absolute position, etc). To facilitate the evaluation of VLMs in the field of remote sensing, we also provide a benchmark evaluation dataset called RSIEval. This dataset consists of human-annotated captions and visual question-answer pairs, allowing for a comprehensive assessment of VLMs in the context of remote sensing. We are actively engaged in expanding the scale of these two datasets to cover a broader spectrum of remote sensing image understanding tasks, further enhancing their utility and applicability. Our dataset and codes will be released at <https://github.com/Lavender105/RSGPT>.

Index Terms—Remote Sensing, Generative Pretrained Transformer (GPT), Large Language Model (LLM), Vision Language Model (VLM)

I. INTRODUCTION

Deep learning models, such as convolutional neural networks (CNNs) [20] and Vision Transformers [13], are capable of automatically learning complex patterns and representations from remote sensing data. It enables accurate and efficient

analysis of large-scale remote sensing datasets and now has become the dominant method for remote sensing data analysis. The use of deep learning in remote sensing has significantly contributed to improved understanding and decision-making in various geo-related applications, including environmental monitoring, agriculture, urban planning, and disaster management [25], [62], [24], [55]. A comprehensive review of deep learning in remote sensing can be found at [85], [74], [37]. Although deep learning methods have achieved success in various remote sensing image analysis tasks, existing deep learning-based models mostly focus on the visual information extraction from remote sensing images, while paying less attention to the semantic understanding of visual tokens and lack of general reasoning abilities [61].

In the past few years, Large language models (LLMs), built from large transformer networks have achieved remarkable performance in natural language understanding and generation tasks, such as language modeling, text generation, and question answering [46]. Of particular note are the advancements showcased by ChatGPT [39] and GPT-4 [40]. These models have showcased astonishing levels of general world knowledge and reasoning capabilities, achieved through extensive learning from vast amounts of textual data. Their achievements in language understanding have significantly contributed to the emergence of what is known as AI2.0. Recent research has witnessed a growing interest in integrating visual models, such as ResNet [15] and ViT [13], with LLMs to create a new class of models referred to as Vision Language Models (VLMs).

VLMs refer to a category of artificial intelligence models that integrate computer vision and natural language processing techniques to achieve a holistic comprehension of visual and textual data. By concurrently analyzing visual and semantic patterns, VLMs possess the capability to discern intricate relationships between visual elements and linguistic information and offer a more comprehensive and human-like ability to understand visual content. In the past few years, researchers have explored VLMs for numerous remote sensing tasks, including image captioning [51], [35], [76], [77], [28], [59], [27], [81], [86], text-based image generation [6], [9], [80], [16], [64], text-based image retrieval [1], [16], [47], [16], [71], [3], [11], [70], [69], [48], visual question answering [33], [82], [8], [8], [2], [5], [67], [68], scene classification [21], [52], [45], [58], [29], etc. A comprehensive review can be found at [61].

While these early attempts have shown the success of applying VLMs to remote sensing, it is still an emerging field with many unsolved challenges. Existing VLMs in the remote sensing field mostly still focus on developing more powerful visual foundation models to better extract more

Yuan Hu and Jianlong Yuan are with the DAMO Academy, Alibaba Group, Beijing, China (email: huyuan826@gmail.com, gongyuan.yjl@alibaba-inc.com). Congcong Wen is with the Department of Electrical and Computer Engineering, New York University Abu Dhabi, Abu Dhabi, UAE (email: wence@nyu.edu). Xiaonan Lu is with the University of Chinese Academy of Sciences, Beijing, China (email: luxiaonan96@gmail.com). Xiang Li is with the King Abdullah University of Science and Technology, Jeddah, Saudi Arabia (email: xiangli92@ieee.org).

[†] The authors contributed equally to this work.

* Corresponding author: Xiang Li.

representative and robust visual features from remote sensing images (RSIs), thus lacking general reasoning abilities that are emergent in LLMs. Another challenging issue that impedes the development of VLMs in remote sensing is the lack of large-scale aligned image-text datasets. Existing RSI datasets mostly focus on visual recognition tasks and do not provide language annotations. Only a few attempts [44], [44], [10], [79] tried to build image-text RSI datasets but data scale and quality are far from expected.

Recent work [83] indicates that when training LLMs, not only data quantity but rather prompt diversity and response quality really matter for building a high-performance LLM. Their experiments show that finetuning a 65B parameter LLaMA on a small-scale high-quality dataset with only 1,000 prompt-response can lead to a remarkably strong performance, comparable with GPT-4.

Inspired by this exciting finding [83], we build a high-quality Remote Sensing Image Captioning dataset (**RSICap**) to facilitate the construction of large vision language models in the remote sensing field. Note that concurrent work [79] builds a large-scale remote sensing vision-language dataset with 5 million aligned image-text pairs from model-generated captions. In contrast, our RSICap dataset collects 2,585 human-annotated captions with high-quality and rich information. Instead of using short descriptions like the previous dataset, our RSICap dataset provides human-annotated detailed descriptions for each image, covering scene descriptions (e.g., residential area, airport, or farmland), object information (color, shape, counting, absolute position), object relationship (e.g., relative position), and also visual reasoning knowledge (e.g., image capture season). This high-quality dataset facilitates finetuning existing large VLMs to build domain-specific VLMs in remote sensing. We also provide an evaluation dataset (**RSIEval**) dataset that can be used for the evaluation of domain-specific or general VLMs. RSIEval consists of 100 human-annotated captions and 936 visual question-answer pairs with rich information and open-ended questions and answers. We target building a standard benchmark that covers diverse remote sensing image understanding tasks, including image captioning, visual question answering, visual grounding, etc. In the current version, we benchmark two tasks, i.e., image captioning and visual question answering, using cutting-edge VLMs on our RSIEval dataset.

Recent work MiniGPT-4 [84] shows the possibility of training a single projection layer can well align visual features with LLMs and the model shows powerful visual and language understanding capabilities like GPT-4 and also new emerging capabilities including writing stories and poems. Inspired by the great success of MiniGPT-4 [84], we develop a Remote Sensing Generative Pretrained Model (**RSGPT**) based on finetuning InstructBLIP [12] on our newly created RSICap dataset. By finetuning only the Q-Former network and the linear layer of InstructBLIP, our model can quickly learn to align visual features of remote sensing images with LLMs in a data-efficient way. Our RSGPT model shows better image captioning and visual question-answering performance than previous SOTA methods.

II. RELATED WORK

A. GPT

Generative Pre-trained Transformer (GPT) is currently the most popular and successful model in natural language processing and computer vision. The first version of GPT [46] model developed by OpenAI, is one of the pioneering works that explore large transformer networks for diverse natural language processing tasks. By training on web-scale text datasets, this model achieved impressive performance on a wide range of language modeling and text generation tasks. Following the great success of the GPT model, GPT-2 further increased the model capacity to 1.5 billion parameters and demonstrated zero-shot task transfer capabilities on diverse natural language processing (NLP) tasks, including language translation, summarization, question answering, and text completion. Furthermore, in GPT-3 [7], the authors developed a Transformer-based language model with 175 billion parameters and demonstrated that task-agnostic, few-shot performance can be improved by scaling up large language models. GPT-3 also inspired research enthusiasm in in-context learning where a model generates predictions based on previous instructions or prompts. Although previous GPT models can solve various NLP tasks, they generally failed to generate human-desired output. To solve this issue, InstructGPT [42], also known as GPT-3.5 further finetune the GPT-3 model with reinforcement learning from human feedback. Their results demonstrated that instruction finetuning from human feedback can properly align language models with human intent. It is worth mentioning that GPT-3.5 is the model utilized for constructing the widely used ChatGPT platform. Unlike ChatGPT which can only perform language generation, the latest version, GPT-4 [40] not only improves the performance on language generation but also shows promising performance for vision understanding tasks. Inspired by the great success of GPT-based models, other open-source LLMs like OPT [75], LLaMA [54], MOSS [41], and GLM [72] have also demonstrated remarkable performance and made substantial contributions to the field.

B. Vision language models

There has been a remarkable increase in interest in expanding large language models into multi-modal versions. Flamingo [4], for instance, integrates visual adaptation layers into an LLM and is trained on a large-scale interleaved image-text dataset. ML-MFSL [38] is similar to Flamingo, where a visual prefix is introduced as a learnable feature to extract information related to text from the image. After enhancing the visual prefix with the meta mapper network and concatenating it with textual features, LLM is employed to predict the responses. MM-GPT [14] and Otter [22] are fine-tuned on meticulously constructed instruction data to enhance user interaction. BLIP-2 [23] utilizes multiple vision-language losses to align visual features with text via the Q-Former model, and tunes a simple fully connected layer to feed the queried embedding to a frozen language model. Based on BLIP-2, MiniGPT4 [84], mPLUG-OWL [66], and InstructBLIP [12] retain the Q-Former model, replace the language model with a

larger one, and fine-tune on meticulously collected instruction data. In addition, simpler and more direct methods, such as LLaVA [31], directly feed visual features to the LLM using only a learnable fully connected layer. Recent notable advancements in extending LLMs to vision are exemplified by models like KOSMOS-1 [19], KOSMOS-2 [43]. Previous methods primarily focused on general natural images. However, due to the differences in imaging mechanisms and shooting angles between remote sensing images and natural images, these methods perform poorly in the field of remote sensing. Therefore, unlike previous methods, our proposed method focuses on remote sensing and aims to design a visual language model specifically tailored for the remote sensing.

C. Related datasets

UCM-Captions [44] and Sydney-Captions [44] were the earliest remote sensing image caption datasets, constructed based on the UCM dataset [65] and Sydney dataset [73], respectively. UCM-Captions includes 2,100 images and 10,500 captions, whereas Sydney-Captions contains 613 images and 3,065 captions. Subsequently, the RSICD [36] and NWPU-Captions [10] were proposed, which have more image-caption pairs and a greater diversity of scene categories. Specifically, RSICD includes 10,921 images and 54,605 captions, of which there are only 24,333 distinct captions. NWPU-Captions includes 31,500 images and 157,500 captions. Each image in these datasets is annotated with five short captions, but the differences among them are relatively small, and the level of detail is limited to rough descriptions of the main scenes. Concurrent work [79] introduced a large-scale remote sensing vision-language dataset with 5 million aligned image-text pairs, called RS5M. The RS5M dataset was created by carefully filtering RS-related images from publicly available datasets, including LAION400M [49] and CC3 [50], and utilizing the BLIP2 model [23] for automatic image caption generation. In contrast, our RSICaps dataset offers several notable advantages over the RS5M dataset. Firstly, rather than relying on model-generated captions, the RSICaps dataset provides high-quality human-annotated captions. These human annotations offer a higher level of accuracy compared to model-generated pseudo labels. It is worth mentioning that even the most advanced image captioning models of today are still unable to match the performance of human annotators in captioning tasks. Secondly, the RSICap dataset surpasses the RS5M dataset in terms of caption detail. While RS5M has an average caption length of 40 vocabularies, our RSICap dataset offers more extensive and detailed captions, with an average length of 60 vocabularies. This increased level of detail proves beneficial as model-generated captions often struggle with accurately conveying object counts, spatial relationships, and external knowledge that cannot be inferred from the images alone. For instance, a human annotator can easily discern the season in which a remote sensing image was captured based on the yellowing of tree leaves. However, the BLIP2 model would find it challenging to predict such specific information.

III. DATASET CONSTRUCTION

With the pre-training of large language models on massive amounts of text data, they have acquired a wealth of knowledge and expressive abilities. As a result, only a small amount of high-quality data is needed to align these large language models to specific domains. For example, [83] demonstrated remarkably strong performance by fine-tuning LLaMa 65B [54] on just 1,000 high-quality samples. [84] achieved significant improvement on the response reliability and fluency by conducting alignment training on just 3,500 high-quality samples for vision-language domain in the second stage. Based on these findings, we construct **RSICap** dataset by carefully curating 2,585 high-quality remote sensing (RS) image-text pairs to transfer general vision-language models (VLMs) to the RS domain. We also construct an evaluation set **RSIEval** to assess the models' ability on remote sensing image captioning (RSIC) and remote sensing visual question answering (RSVQA) tasks.

A. RSICap

1) *Dataset Curating*: We construct RSICap based on DOTA object detection dataset. We choose DOTA dataset for three reasons: (1) DOTA dataset provides rich image diversity, including images from different satellite and aerial sensors such as GF-2, JL-1 and Google Earth satellite images, and aerial images with different resolutions. Additionally, DOTA includes both color and panchromatic images; (2) DOTA dataset contains diverse scenes. DOTA-v1.5, which we used in this paper, covers 16 object categories; (3) DOTA provides category and bounding box labels, which facilitates the statistical counting of interested objects. Training with images of diverse sensors and scenes benefits the generalization ability of VLMs.

The original size of images in DOTA ranges from 800×800 to $4,000 \times 4,000$. We divided the images in the training set into patches with a size of 512×512 and then random selected a total of 2,585 patches. Five remote sensing experts annotated the images. The caption annotation procedure follows the principles of: (1) describing image attributes, including satellite/aerial images, color/panchromatic images, and high/low resolution; (2) describing object attributes, including object quantity, color, shape, size, and spatial position (including absolute position in the image and relative position between objects); (3) generally, the annotation process involves first describing the overall scene of the image, followed by describing specific objects. Following the principles, we generate 2,585 high-quality RS image-text pairs. Figure 1 presents an example of RSICap. The caption provides a description of the scene with rich and specific details, which can provide valuable reference for user interaction of remote sensing knowledge through VLMs.

2) *Qualitative Analysis*: We first compare RSICap with previous RS image caption datasets in Figure 1, including UCM-Captions [44], Sydney-Captions [44], RSICD [36], NWPU-Captions [10] and RS5M [79]. All previous datasets have captions consisting of 5 short sentences, each describing only the main scene without much detail, and the content expressed

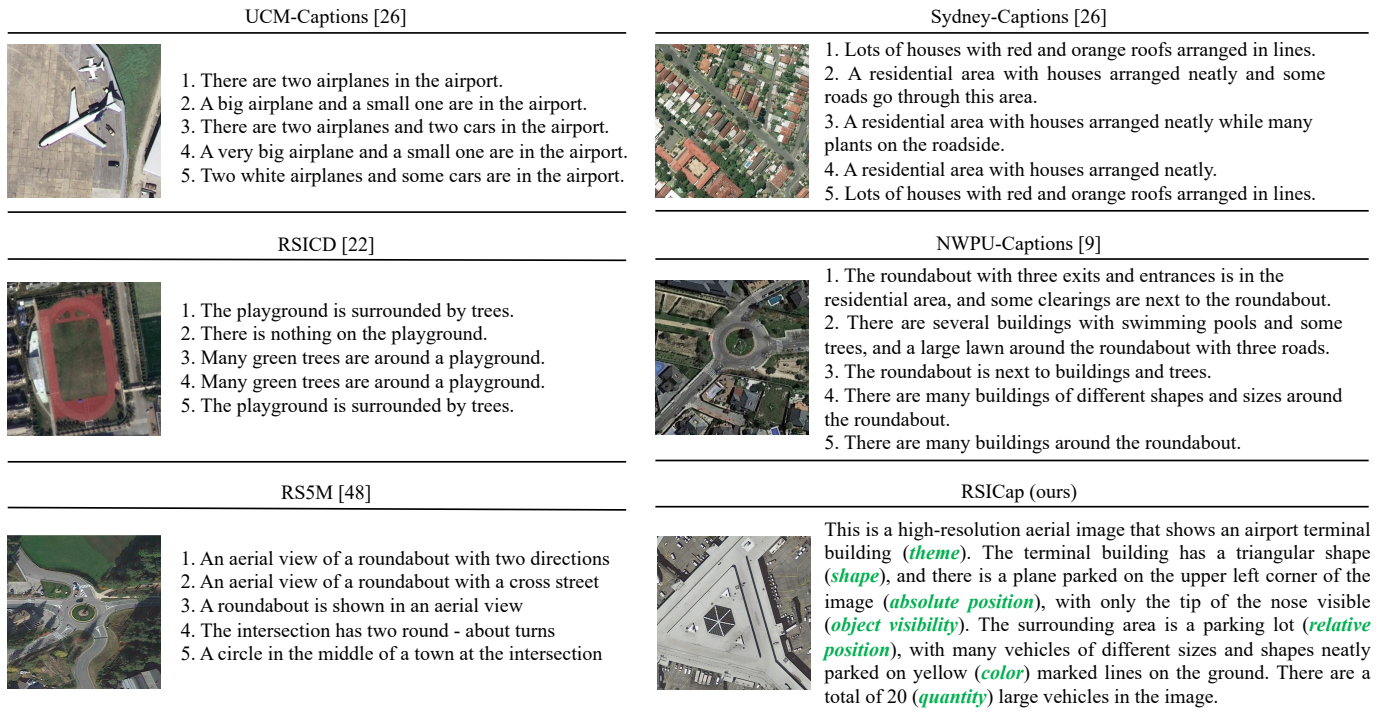


Fig. 1. Qualitative comparison among UCM-Captions [44], Sydney-Captions [44], RSICD [36], NWPU-Captions [10], RS5M [79] and RSICap (ours). The caption of our dataset provides much more details compared to that of other datasets, including theme (airport), quantity (20 vehicles), color (yellow marked lines), shape (triangular terminal building), absolute position (the plane is parked on the upper left corner of the image), relative position (the surrounding area of the terminal is a parking lot) and description of object visibility (with only the tip of the nose visible).

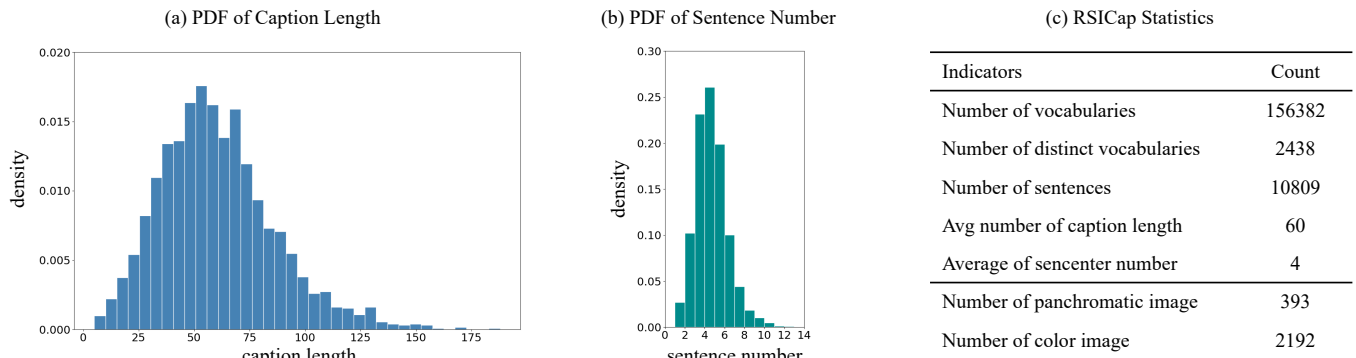


Fig. 2. Quantitative analysis of the RSICap dataset. (a) Probability density function (PDF) of caption length. (b) PDF of the sentence number. (c) Statistical indicators of the RSICap dataset.

in different sentences is very similar. It is worth mentioning that NWPU-Caption’s captions have some descriptions of relative positions, while our dataset RSICap is more diverse and includes descriptions of both the main scene and object details (including quantity, color, shape, absolute position, and relative position). The example of RS5M in Figure 1 shows captions generated by the pre-trained vision-language model BLIP-2 [23], but the correctness and diversity of the generated results are far inferior to the manual annotated descriptions of our dataset.

We next visualize the resolution diversity, scene diversity, and reasonable speculation in our dataset. Figure 7 (a) shows

the resolution diversity of our dataset, including aerial image, color satellite image, panchromatic satellite image, and low-resolution, low-contrast panchromatic satellite image. Figure 7 (b) shows the scene diversity of our dataset, including airport, harbor, tennis court, and residential area. In addition to these scenes, the dataset also covers industrial area, commercial area, farmland, overpass, urban streets, and scenes without a specific main scene that contains multiple elements. Figure 7 (c) shows that we make reasonable speculation in caption writing, such as speculating that the scene is an airport and its surroundings from the combination of multiple typical elements such as a large parking lot, railway tracks, and



Image	Question	Answer
	<p>Q: Does this image contains roundabout? (presence)</p> <p>Q: Does this image contains buildings? (presence)</p> <p>Q: How many cars are there in this image? (quantity)</p> <p>Q: What color are the parking lines in the parking lot? (color)</p> <p>Q: Where is the parking lot with only three cars located in the image? (absolute position)</p> <p>Q: What is the relative position between the parking lots and the roundabout? (relative position)</p> <p>Q: Is this image a panchromatic image or a color image? (panchromatic/color)</p> <p>Q: Is the resolution of this image high or low? (image resolution)</p>	<p>A: Yes.</p> <p>A: No.</p> <p>A: Sixty-eight.</p> <p>A: White.</p> <p>A: Upper left corner.</p> <p>A: The parking lots are located on the left side of the roundabout.</p> <p>A: Color image.</p> <p>A: High.</p>
	<p>Q: Does this image contains ships? (presence)</p> <p>Q: Does this image contains buildings? (presence)</p> <p>Q: How many ships are there in this image? (quantity)</p> <p>Q: What is the color of the water in the image? (color)</p> <p>Q: Where is the ship located in the image? (absolute position)</p> <p>Q: Is the ship in the image in motion or stationary? (reason)</p> <p>Q: Is the ship in the image moving fast or slow? (reason)</p>	<p>A: Yes.</p> <p>A: No.</p> <p>A: One.</p> <p>A: Green.</p> <p>A: Lower part.</p> <p>A: In motion.</p> <p>A: Fast.</p>

Fig. 3. Examples of image-question-answer triplets in RSIEval. These questions and answers are very diverse, with examples shown in the figure including presence, quantity, color, absolute position, relative position, panchromatic/color image, image resolution, and visual reasoning, along with their corresponding open-ended answers. Question types are indicated in parentheses and highlighted in green.

airplanes; from the appearance of a plane in the farmland, speculating that the scene was captured by the satellite when the plane was passing over the farmland; speculating that the season was autumn or winter from trees with visible trunks only; speculating that the scene is a part of an airport from a partially visible airplane. The descriptions of making reasonable speculation based on the visual content helps to empower the model with a certain ability for RS-related knowledge reasoning.

3) *Quantitative Analysis*: We then present some quantitative statistical results on our RSICap dataset. Figure 2 (a) displays the probability density function (PDF) of caption length, which takes on a shape similar to a normal distribution. The longest caption length contains 188 vocabularies, with an average length of 60 vocabularies, making it longer than all previous RS image caption datasets. Figure 2 (b) illustrates the PDF of the sentence number, with the longest containing 13 sentences and an average of 4 sentences per caption. Figure 2 (c) shows several statistical indicators of our RSICap dataset, such as the total number of vocabularies in captions being 156,382, the number of distinct vocabularies being 2,438, and the total number of sentences being 10,809. Additionally, the ratio of panchromatic imagery to colored imagery is approximately 1:5.8.

B. RSIEval

In order to benchmark various domain-specific and general VLMs on remote sensing image caption (RSIC) and remote sensing visual question answering (RSVQA) tasks, we construct an evaluation set **RSIEval**. We divided the images in the validation set of DOTA-v1.5 into patches with a size of 512×512 and then selected 100 images from these patches for further manual annotation. Five RS experts participated in the annotation. For benchmarking RSIC task, we created the captions for the 100 images following the principles mentioned in the previous sub-section. For benchmarking RSVQA task, question-answer pairs are generated for each image. The questions fall into four categories: object-related

questions, image-related questions, scene-related questions, and reasoning-related questions. Object-related questions include presence, quantity, color, absolute position, relative position, area comparison and road direction. Image-related questions include high/low resolution, and panchromatic/color image. Scene-related questions include main theme/scene, and urban/rural scene. Reasoning-related questions include “What season was this image taken in?”, “Is the area shown in the image dry?”, “Is the ship in the image moving fast or slow?”, “Is the water surface in the image calm or wavy?”, and so on. These questions require the model to have a certain level of visual reasoning ability, that is, generating the answers based on the image content and external knowledge. As these questions are open-ended, we manually wrote answers to the questions. Figure 3 shows two examples of image-question-answer triplets in RSIEval. RSIEval provides the most diverse set of questions and answers to date, compared to existing RSVQA datasets such as RSVQA [33], RSIVQA [82], and RSVQA×BEN [32]. In summary, RSIEval consists of 100 high-quality image-caption pairs with one caption per image, and 936 diverse image-question-answer triplets with an average of 9 questions per image.

IV. METHOD

A. Network Structure

RSGPT is a pre-training method designed for efficient and generic remote sensing (RS) vision-language tasks. As shown in Figure 4, off-the-shelf frozen pre-trained image encoders (EVA-G) and large language models (vicuna7b, vicuna13b) form the foundation of the model. Following InstructBLIP, an instruction-aware Query Transformer (Q-Former) is inserted between them to enhance the alignment representation of visual features and textual features. Specifically, the Q-Former extract visual features from the frozen pre-trained image encoder, with K learnable query embeddings interacting with the encoder’s output through cross-attention. This enables RSGPT to extract comprehensive visual features that are essential for RS vision-language tasks. Moreover, the instruction-aware

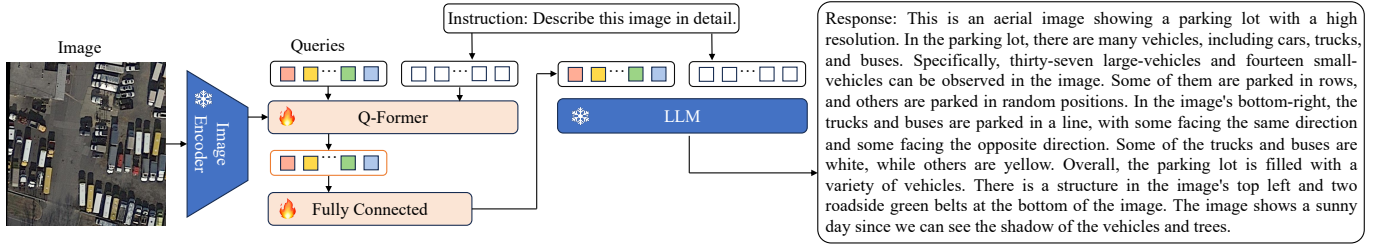


Fig. 4. Overview architecture of RSGPT. It consists of an image encoder, an instruction-aware Q-Former, a fully connected layer, and a large language model (LLM). The image encoder and LLM is frozen, only the Q-Former and the linear layer are trained for adapting the model to the remote sensing domain.

mechanism that takes in instruction text tokens as additional input and interact the text tokens with the query embeddings through self-attention layers, enables the Q-Former to extract task-relevant image features. Furthermore, a linear layer is introduced to project the output features of the Q-Former into the input features of LLM. In the end, the LLM produces the final response based on the visual information and textual prompts. The LLM in RSGPT is pre-trained on a large corpora of text data, which allows it to generate accurate and fluent responses. The combination of pre-trained image encoders, Q-Former, linear layer, and large language models makes RSGPT a powerful pre-training method for RS vision-language tasks.

B. Training Strategy

During training, in order to leverage the ability of pre-trained models on large amounts of general visual images and improve training efficiency, we adopt the strategy of loading pre-trained weights and fine-tuning part of network for training our RSGPT. We observed that InstructBLIP, that trained on visual spatial reasoning tasks, exhibits a certain level of spatial understanding, which is a crucial aspect for accurately describing the object positions in remote sensing images. Consequently, we integrated the pre-trained weights of InstructBLIP into RSGPT. It should be noted that InstructBLIP is trained on 26 datasets across 11 different tasks, including image captioning, visual question answering, and visual reasoning for vision-language representation learning. In order to make our model adapt to remote sensing images, we subsequently fine-tune the Q-Former and linear layer in RSGPT using the proposed high-quality RSICap dataset. During fine-tuning, some well-designed instructions such as "Describe this image in detail." are utilized. This enabled the model to handle RS tasks with multiple modalities.

V. EXPERIMENTS

A. Experimental Details

RSGPT is initialized with InstructBLIP pretrained weights. During the finetuning stage, we only train the model for 5 epochs with a batch size of 64. We adopt the AdamW optimizer with $\beta_1 = 0.9$, $\beta_2 = 0.999$, and weight decay of 0.05. Additionally, we set the initial learning rate to $3e-5$, and warmup the learning rate for 1 epoch. Cosine policy is adopted for the decay schedule. All models were trained using 8 NVIDIA A100 GPUs.

Dimension	Level	Description
Detail	A	The caption has comprehensive and rich details, describing almost all types of objects in the ground truth.
	B	The caption has rich details, describing most types of objects and their attribute information.
	C	The caption has only a small amount of details, describing a few types of objects and their attribute information.
	D	The caption has no detail descriptions.
Position	A	The caption has rich position descriptions for objects and all are correct.
	B	The caption has rich position descriptions for objects with an accuracy higher than 50%.
	C	The caption has few position descriptions, or rich position descriptions but with an accuracy less than 50%.
	D	The caption has no position descriptions.
Hallucination	A	The caption has no hallucination description.
	B	The caption has hallucination description, and it accounts for less than 50%
	C	The caption has a large proportion of hallucination description, more than 50%
	D	The caption is entirely hallucination description.

Fig. 5. The four-level rating system for scoring the quality of the generated remote sensing image captions from three dimensions, namely detail description, position description, and hallucination description.

B. Benchmark evaluation

We first compare RSGPT with three vision-language models, namely BLIP2 [23], MiniGPT4 [84], and InstructBLIP [12] on the proposed evaluation set RSIEval. We evaluate the performance of the four models on the remote sensing image captioning (RSIC) and remote sensing visual question answering (RSVQA) tasks by manual scoring, due to the open-ended responses of the models.

1) *RSIC*: Under the instruction "Please provide a detailed description of the image", each model generated a corresponding caption for 100 images in RSIEval. We score the generated image captions from three dimensions, namely detail description, position description, and hallucination description. We adopt a four-level rating system to rate each dimension as A, B, C, or D, following [60], [66]. The criteria for each level are shown in Figure 5. The scoring results of the four models are presented in Figure 6. As can be seen from the detail score in Figure 6 (a), RSGPT achieves the best performance with

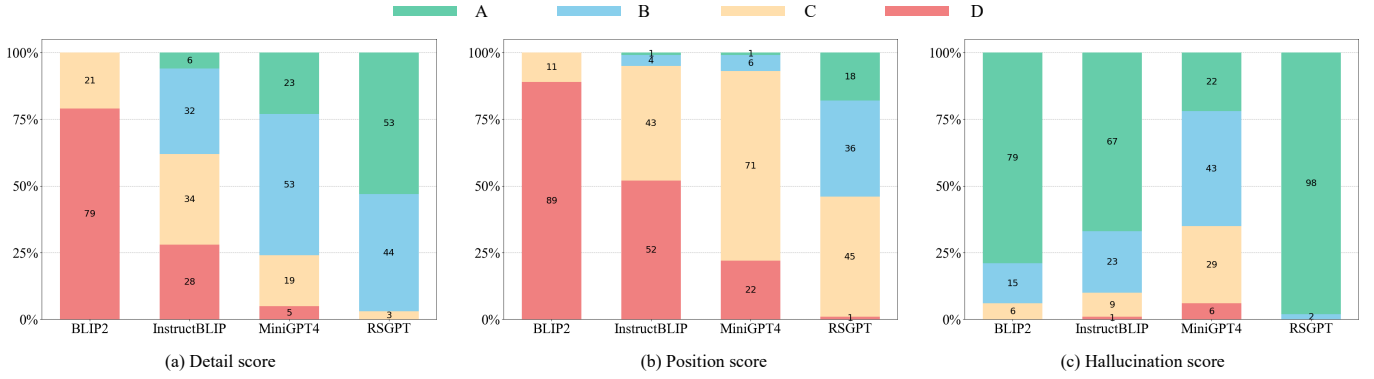


Fig. 6. The comparison among RSGPT, BLIP2, InstructBLIP, and MiniGPT4 on the proposed RSIEval image captioning test set. The scores are manual evaluated from three dimensions, namely detail description, position description, and hallucination description, as shown in (a), (b), and (c), respectively. Each dimension is rated as A, B, C or D, according to the criteria shown in Figure 5.

Method	Presence	Quantity	Color	Absolute pos.	Relative pos.	Area comp.	Road dir.	Image	Scene	Reasoning	Avg accuracy
BLIP2	60.41	26.02	43.24	7.69	13.16	58.14	33.33	74.42	43.24	47.50	45.56
MiniGPT4	29.70	9.76	31.53	1.54	1.32	16.28	0.00	34.88	24.32	17.50	21.82
InstructBLIP	76.14	21.95	45.05	12.31	10.53	69.77	0.00	81.40	45.95	57.50	53.26
RSGPT (ours)	81.22	39.02	54.05	38.46	35.53	62.79	66.67	93.02	89.19	70.00	65.24

TABLE I

COMPARISON WITH PREVIOUS VISION-LANGUAGE MODELS ON THE RSVQA TEST SET OF RSIEVAL. ALL ACCURACY SCORES ARE MEASURED BY %.

Method	BLIP2	MiniGPT4	InstructBLIP	RSGPT (ours)
Quantity Relative Error	32.6718	0.8548	0.7318	0.4828

TABLE II

QUANTITY RELATIVE ERROR COMPARISON WITH PREVIOUS VISION-LANGUAGE MODELS ON THE RSVQA TEST SET OF RSIEVAL.

53 A, 44 B, and 3 C, followed by MiniGPT4, InstructBLIP, and BLIP2. BLIP2 has the lowest detail score with 79 D and 21 C. Figure 8 also indicates that BLIP2’s predicted captions only consist of a brief description of the main scene without more detailed descriptions. As shown in Figure 6 (b), regarding the position score, RSGPT obtains the most A with 18, while MiniGPT4, InstructBLIP, and BLIP2 have 1, 1, and 0, respectively. Figure 8 also demonstrates that, except for RSGPT, other models rarely describe the positions of objects and their relative positioning with other objects, resulting in more C and D scores. Figure 6 (c) shows the hallucination scoring results, and except for MiniGPT4, all other models received the most A, among which RSGPT had the highest A score of 98. MiniGPT4’s generated captions have a relatively higher proportion of hallucination descriptions, such as the sky, clouds, pedestrians, and other objects that cannot be observed in remote sensing imagery, as shown in Figure 8. InstructBLIP occasionally has descriptions of people or pedestrians, while BLIP2 seldom has hallucination descriptions due to its brief descriptions. RSGPT demonstrates the best performance and seldom describes irrelevant objects.

2) *RSVQA*: Next, we evaluated the performance of the four models on the RSIEval VQA test set. Firstly, we divided the 936 questions in the test set into 10 categories, including presence, quantity, color, absolute position, relative position,

area comparison, road direction, image, scene, and reasoning. The first seven categories belong to object-level questions, while the latter three correspond to image-level, scene-level, and reasoning-level questions, as described in section III-B. We calculated the accuracy for each question type and the average accuracy for all types, as shown in Table I. RSGPT outperformed other models in almost all question types, with an average accuracy 11.98%, 19.68%, and 43.42% higher than InstructBLIP, BLIP2, and MiniGPT4, respectively. RSGPT performed well in presence, image, and scene-related questions, but poorly in quantity, absolute position, and relative position-related questions, indicating that these types of questions are more challenging and require stronger object recognition capabilities of the model. In addition, for quantity-related questions, the impact of prediction errors differs for scenarios with a large number of objects, such as hundreds of cars in a parking lot, versus scenarios with a small number of objects, such as a few airplanes near a terminal. Therefore, in addition to simply judging the correctness of the quantity prediction, we also calculated the relative error of the quantity prediction, as shown in Table II. The table shows that RSGPT has the smallest relative error, while BLIP2 has the largest, significantly higher than the other three models, indicating that BLIP2’s ability to predict quantity is poor. Figure 9 and Figure 10 present the predicted results of the four models on some types of questions.

C. Comparison with SOTA

In this sub-section, we compare RSGPT with state-of-the-art methods across three existing remote sensing image captioning (RSIC) datasets and two existing remote sensing visual question answering (RSVQA) datasets.

Method	BLEU-1	BLEU-2	BLEU-3	BLEU-4	METEOR	ROUGE_L	CIDEr
VLAD + RNN [36]	63.11	51.93	46.06	42.09	29.71	58.78	200.66
VLAD + LSTM [36]	70.16	60.85	54.96	50.30	34.64	65.20	231.31
mRNN [44]	60.10	50.70	32.80	20.80	19.30	-	214.00
mLSTM [44]	63.50	53.20	37.50	21.30	20.30	-	222.50
mGRU [26]	42.56	29.99	22.91	17.98	19.41	37.97	124.82
mGRU embedword [26]	75.74	69.83	64.51	59.98	36.85	66.74	279.24
CSMLF [56]	37.71	14.85	7.63	5.05	9.44	29.86	13.51
SAA [34]	79.62	74.01	69.09	64.77	38.59	69.42	294.51
Soft-attention [63]	74.54	65.45	58.55	52.50	38.86	72.37	261.24
Hard-attention [63]	81.57	73.12	67.02	61.82	42.63	76.98	299.47
SD-RSIC [53]	74.80	66.40	59.80	53.80	39.00	69.50	213.20
RTRMN (semantic) [57]	55.26	45.15	39.62	35.87	25.98	55.38	180.25
RTRMN (statistical) [57]	80.28	73.22	68.21	63.93	42.58	77.26	312.70
SVM-D BOW [17]	76.35	66.64	58.69	51.95	36.54	68.01	271.42
SVM-D CONC [17]	76.53	69.47	64.17	59.42	37.02	68.77	292.28
Post-processing [18]	79.73	72.98	67.44	62.62	40.80	74.06	309.64
RSGPT (ours)	86.12	79.14	72.31	65.74	42.21	78.34	333.23

TABLE III

COMPARISON WITH STATE-OF-THE-ARTS ON THE UCM-CAPTIONS DATASET. ALL ACCURACY SCORES ARE MEASURED BY %.

Method	BLEU-1	BLEU-2	BLEU-3	BLEU-4	METEOR	ROUGE_L	CIDEr
VLAD + RNN [36]	56.58	45.14	38.07	32.79	26.72	52.71	93.72
VLAD + LSTM [36]	49.13	34.12	27.60	23.14	19.30	42.01	91.64
mRNN [44]	51.30	37.50	20.40	19.30	18.50	-	161.00
mLSTM [44]	54.60	39.50	22.30	21.20	20.50	-	186.00
mGRU [26]	69.64	60.92	52.39	44.21	31.12	59.17	171.55
mGRU embedword [26]	68.85	60.03	51.81	44.29	30.36	57.47	168.94
CSMLF [56]	59.98	45.83	38.69	34.33	24.75	50.18	75.55
SAA [34]	68.82	60.73	52.94	45.39	30.49	58.20	170.52
Soft-attention [63]	73.22	66.74	62.23	58.20	39.42	71.27	249.93
Hard-attention [63]	75.91	66.10	58.89	52.58	38.98	71.89	218.19
SD-RSIC [53]	72.40	62.10	53.20	45.10	34.20	63.60	139.50
SVM-D BOW [17]	77.87	68.35	60.23	53.05	37.97	69.92	227.22
SVM-D CONC [17]	75.47	67.11	59.70	53.08	36.43	67.46	222.22
Post-processing [18]	78.37	69.85	63.22	57.17	39.49	71.06	255.53
RSGPT (ours)	82.26	75.28	68.57	62.23	41.37	74.77	273.08

TABLE IV

COMPARISON WITH STATE-OF-THE-ARTS ON THE SYDNEY-CAPTIONS DATASET. ALL ACCURACY SCORES ARE MEASURED BY %.

Method	BLEU-1	BLEU-2	BLEU-3	BLEU-4	METEOR	ROUGE_L	CIDEr
VLAD + RNN [36]	49.38	30.91	22.09	16.77	19.96	42.42	103.92
VLAD + LSTM [36]	50.04	31.95	23.19	17.78	20.46	43.34	118.01
mRNN [44]	45.58	28.25	18.09	12.13	15.69	31.26	19.15
mLSTM [44]	50.57	32.42	23.29	17.46	17.84	35.02	31.61
mGRU [26]	42.56	29.99	22.91	17.98	19.41	37.97	124.82
mGRU embedword [26]	60.94	46.24	36.80	29.81	26.14	48.20	159.54
CSMLF [56]	57.59	38.59	28.32	22.17	21.28	44.55	52.97
SAA [34]	59.35	45.11	35.29	28.08	26.11	49.57	132.35
Soft-attention [63]	65.13	49.04	39.00	32.30	26.39	49.69	90.58
SD-RSIC [53]	64.50	47.10	36.40	29.40	24.90	51.90	77.50
RTRMN (semantic) [57]	62.01	46.23	36.44	29.71	28.29	55.39	151.46
RTRMN (statistical) [57]	61.02	45.14	35.35	28.59	27.51	54.52	148.20
SVM-D BOW [17]	61.12	42.77	31.53	24.11	23.03	45.88	68.25
SVM-D CONC [17]	59.99	43.47	33.55	26.89	22.99	45.57	68.54
MLAT [30]	66.90	51.13	41.14	34.21	27.31	50.57	94.27
Post-processing [18]	62.90	45.99	35.68	28.68	25.30	47.34	75.56
RSGPT (ours)	70.32	54.23	44.02	36.83	30.10	53.34	102.94

TABLE V

COMPARISON WITH STATE-OF-THE-ARTS ON THE RSICD DATASET. ALL ACCURACY SCORES ARE MEASURED BY %.

1) *RSIC*: Three different datasets, namely UCM-captions [44], Sydney-captions [44], and RSICD [36], are included in the RSIC comparison experiments. UCM-captions contains 2,100 high-resolution remote sensing images and 10,500 caption descriptions. Sydney-captions contains 613 images and

3,065 caption descriptions. RSICD contains 10,921 images and 54,605 captions. All three datasets have 5 descriptions for each image. As the caption descriptions in these datasets are very short and limited in vocabulary, we fine-tuned RSGPT on these datasets to generate output results with similar length

Method	Presence	Comparison	Average Accuracy
RSVQA [33]	90.43	88.19	89.31
EasyToHard [67]	91.39	89.75	90.57
Bi-Modal [5]	92.03	91.83	91.93
SHRNet [78]	92.45	91.68	92.07
RSGPT (ours)	91.86	92.15	92.00

TABLE VI

COMPARISON WITH STATE-OF-THE-ARTS ON TEST SET 1 OF RSVQA-HR DATASET. ALL ACCURACY SCORES ARE MEASURED BY %.

Method	Presence	Comparison	Average Accuracy
RSVQA [33]	86.26	85.94	86.10
EasyToHard [67]	87.97	87.68	87.83
Bi-Modal [5]	89.37	89.62	89.50
SHRNet [78]	89.81	89.44	89.63
RSGPT (ours)	89.87	89.68	89.78

TABLE VII

COMPARISON WITH STATE-OF-THE-ARTS ON TEST SET 2 OF RSVQA-HR DATASET. ALL ACCURACY SCORES ARE MEASURED BY %.

and vocabulary as the ground truth captions. Specifically, we fine-tuned RSGPT for 5, 5, and 15 epochs on the training sets of UCM-captions, Sydney-captions, and RSICD, respectively, and evaluated on the corresponding test sets. The evaluation metrics used are typical metrics for image captioning, including BiLingual Evaluation Understudy (BLEU), Recall-Oriented Understudy for Gisting Evaluation (ROUGE_L), Metric for Evaluation of Translation with Explicit Ordering (METEOR), and Consensus-based Image Description Evaluation (CIDEr). For BLEU, we used $n=1,2,3,4$ for n -gram precision. Tables III, Table IV, and Table V show the experimental results. As shown in the tables, RSGPT significantly outperforms previous methods on most metrics. For example, on BLEU-1, RSGPT surpasses the previous best method by 4.55%, 3.89%, and 3.42% on the UCM-captions, Sydney-captions, and RSICD datasets, respectively. As can be seen, RSGPT easily surpasses other methods on the existing RSIC datasets with only a few training epochs, demonstrating the powerful ability of large visual-language model.

2) *RSVQA*: RSVQA-HR [33] and RSVQA-LR [33] datasets are utilized for RSVQA comparison experiments. RSVQA-HR [33] contains 10,569 high-resolution images and 1,066,316 question-answer pairs, of which 61.5%, 11.2%, 20.5%, and 6.8% are split into the training set, validation set, test set 1, and test set 2, respectively. There are four question types in this dataset, including presence, comparison, area, and count. RSVQA-LR [33] contains 772 low-resolution images and 77,232 question-answer pairs, of which 77.8%, 11.1%, and 11.1% are used for training, validation, and testing, respectively. The question types include presence, comparison, rural/urban, and count. We fine-tuned RSGPT for 5 epochs on the training sets of RSVQA-HR and RSVQA-LR, and evaluated it on the corresponding test sets. We removed area and count questions during training and testing because the answers to area and count questions are numerical and quantized into multiple categories. For example, in the RSVQA-LR dataset, the answers to counting questions are quantized into the five categories: 0, between 1 and 10, between 11

Method	Presence	Comparison	Rural/Urban	Average Accuracy
RSVQA [33]	87.46	81.50	90.00	86.32
EasyToHard [67]	90.66	87.49	91.67	89.94
Bi-Modal [5]	91.06	91.16	92.66	91.63
SHRNet [78]	91.03	90.48	94.00	91.84
RSGPT (ours)	91.17	91.70	94.00	92.29

TABLE VIII

COMPARISON WITH STATE-OF-THE-ARTS ON THE RSVQA-LR DATASET. ALL ACCURACY SCORES ARE MEASURED BY %.

and 100, between 101 and 1000, and more than 1000. In addition, we constrained the maximum and minimum lengths of RSGPT’s answers to 5 and 2 characters, respectively, because for presence and comparison questions, the ground-truth answers are only “yes” or “no”, and for rural/urban questions, the ground-truth answers are only “rural” or “urban”. Table VI and Table VII show the experimental results on RSVQA-HR test set 1 and test set 2, respectively. The accuracy of each question type and the average accuracy are reported in the tables. On test set 1, RSGPT achieved comparable results to the previous best method SHRNet [78], while on test set 2, RSGPT outperformed SHRNet on all metrics. Table 3 shows the results on the RSVQA-LR test set, where RSGPT outperformed previous methods on all metrics. As shown, RSGPT can match or even surpass the SOTA method with only 5 epochs of fine-tuning. Experiments on 5 datasets of RSIC and RSVQA tasks demonstrated the effectiveness and superiority of RSGPT on multiple vision-language related tasks.

VI. CONCLUSION

In this paper, we propose a high-quality dataset, RSICap, to facilitate the development of visual-language models in the field of remote sensing (RS). RSICap contains 2,585 manually annotated image captions, each of which provides detailed descriptions of the image scene, as well as object information such as color, shape, position, and quantity. It is the most information-rich dataset in the RS field to date, with the longest caption length (an average of 60 vocabularies per caption). In addition, we also manually annotated an evaluation set, RSIEval, which includes 100 image-caption pairs and 936 visual question-answer pairs, providing a benchmark for the evaluation of visual-language models on the RSIC and RSVQA tasks. We trained a RS visual-language model, RSGPT, on the RSICap dataset, and evaluated it on RSIEval. As the model’s responses are open-ended, we conducted manual scoring on them. The experimental results show that RSGPT outperforms other models significantly in both tasks. Furthermore, we evaluated RSGPT across five existing remote sensing datasets, including two RSIC datasets and three RSVQA datasets, and the experimental results demonstrate that RSGPT outperforms the previous state-of-the-art methods in most metrics.

REFERENCES

- [1] T. Abdullah, Y. Bazi, M. M. Al Rahhal, M. L. Mekhalfi, L. Rangarajan, and M. Zuair. Texts: Deep bidirectional triplet network for matching text to remote sensing images. *Remote Sensing*, 12(3):405, 2020. 1

- [2] M. M. Al Rahhal, Y. Bazi, S. O. Alsaleh, M. Al-Razgan, M. L. Mekhalfi, M. Al Zuair, and N. Alajlan. Open-ended remote sensing visual question answering with transformers. *International Journal of Remote Sensing*, 43(18):6809–6823, 2022. 1
- [3] M. M. Al Rahhal, Y. Bazi, N. A. Alsharif, L. Bashmal, N. Alajlan, and F. Melgani. Multilanguage transformer for improved text to remote sensing image retrieval. *IEEE Journal of Selected Topics in Applied Earth Observations and Remote Sensing*, 15:9115–9126, 2022. 1
- [4] J.-B. Alayrac, J. Donahue, P. Luc, A. Miech, I. Barr, Y. Hasson, K. Lenc, A. Mensch, K. Millican, M. Reynolds, et al. Flamingo: a visual language model for few-shot learning. *Advances in Neural Information Processing Systems*, 35:23716–23736, 2022. 2
- [5] Y. Bazi, M. M. Al Rahhal, M. L. Mekhalfi, M. A. Al Zuair, and F. Melgani. Bi-modal transformer-based approach for visual question answering in remote sensing imagery. *IEEE Transactions on Geoscience and Remote Sensing*, 60:1–11, 2022. 1, 9
- [6] M. B. Bejjga, F. Melgani, and A. Vascotto. Retro-remote sensing: Generating images from ancient texts. *IEEE Journal of Selected Topics in Applied Earth Observations and Remote Sensing*, 12(3):950–960, 2019. 1
- [7] T. Brown, B. Mann, N. Ryder, M. Subbiah, J. D. Kaplan, P. Dhariwal, A. Neelakantan, P. Shyam, G. Sastry, A. Askell, et al. Language models are few-shot learners. *Advances in neural information processing systems*, 33:1877–1901, 2020. 2
- [8] C. Chappuis, V. Mendez, E. Walt, S. Lobry, B. Le Saux, and D. Tuia. Language transformers for remote sensing visual question answering. In *IGARSS 2022-2022 IEEE International Geoscience and Remote Sensing Symposium*, pages 4855–4858. IEEE, 2022. 1
- [9] C. Chen, H. Ma, G. Yao, N. Lv, H. Yang, C. Li, and S. Wan. Remote sensing image augmentation based on text description for waterside change detection. *Remote Sensing*, 13(10):1894, 2021. 1
- [10] Q. Cheng, H. Huang, Y. Xu, Y. Zhou, H. Li, and Z. Wang. Nwpucaptions dataset and mlca-net for remote sensing image captioning. *IEEE Transactions on Geoscience and Remote Sensing*, 60:1–19, 2022. 2, 3, 4
- [11] Q. Cheng, Y. Zhou, P. Fu, Y. Xu, and L. Zhang. A deep semantic alignment network for the cross-modal image-text retrieval in remote sensing. *IEEE Journal of Selected Topics in Applied Earth Observations and Remote Sensing*, 14:4284–4297, 2021. 1
- [12] W. Dai, J. Li, D. Li, A. M. H. Tiong, J. Zhao, W. Wang, B. Li, P. Fung, and S. Hoi. Instructblip: Towards general-purpose vision-language models with instruction tuning. *arXiv preprint arXiv:2305.06500*, 2023. 2, 6
- [13] A. Dosovitskiy, L. Beyer, A. Kolesnikov, D. Weissenborn, X. Zhai, T. Unterthiner, M. Dehghani, M. Minderer, G. Heigold, S. Gelly, et al. An image is worth 16x16 words: Transformers for image recognition at scale. *arXiv preprint arXiv:2010.11929*, 2020. 1
- [14] T. Gong, C. Lyu, S. Zhang, Y. Wang, M. Zheng, Q. Zhao, K. Liu, W. Zhang, P. Luo, and K. Chen. Multimodal-gpt: A vision and language model for dialogue with humans. *arXiv preprint arXiv:2305.04790*, 2023. 2
- [15] K. He, X. Zhang, S. Ren, and J. Sun. Deep residual learning for image recognition. In *Proceedings of the IEEE conference on computer vision and pattern recognition*, pages 770–778, 2016. 1
- [16] S. Hochreiter and J. Schmidhuber. Long short-term memory. *Neural computation*, 9(8):1735–1780, 1997. 1
- [17] G. Hoxha and F. Melgani. A novel svm-based decoder for remote sensing image captioning. *IEEE Transactions on Geoscience and Remote Sensing*, 60:1–14, 2021. 8
- [18] G. Hoxha, G. Scuccato, and F. Melgani. Improving image captioning systems with post-processing strategies. *IEEE Transactions on Geoscience and Remote Sensing*, 2023. 8
- [19] S. Huang, L. Dong, W. Wang, Y. Hao, S. Singhal, S. Ma, T. Lv, L. Cui, O. K. Mohammed, Q. Liu, et al. Language is not all you need: Aligning perception with language models. *arXiv preprint arXiv:2302.14045*, 2023. 3
- [20] Y. LeCun, L. Bottou, Y. Bengio, and P. Haffner. Gradient-based learning applied to document recognition. *Proceedings of the IEEE*, 86(11):2278–2324, 1998. 1
- [21] A. Li, Z. Lu, L. Wang, T. Xiang, and J.-R. Wen. Zero-shot scene classification for high spatial resolution remote sensing images. *IEEE Transactions on Geoscience and Remote Sensing*, 55(7):4157–4167, 2017. 1
- [22] B. Li, Y. Zhang, L. Chen, J. Wang, J. Yang, and Z. Liu. Otter: A multi-modal model with in-context instruction tuning. *arXiv preprint arXiv:2305.03726*, 2023. 2
- [23] J. Li, D. Li, S. Savarese, and S. Hoi. Blip-2: Bootstrapping language-image pre-training with frozen image encoders and large language models. *arXiv preprint arXiv:2301.12597*, 2023. 2, 3, 4, 6
- [24] X. Li, C. Wen, L. Wang, and Y. Fang. Geometry-aware segmentation of remote sensing images via joint height estimation. *IEEE Geoscience and Remote Sensing Letters*, 19:1–5, 2021. 1
- [25] X. Li, X. Yao, and Y. Fang. Building-a-nets: Robust building extraction from high-resolution remote sensing images with adversarial networks. *IEEE Journal of Selected Topics in Applied Earth Observations and Remote Sensing*, 11(10):3680–3687, 2018. 1
- [26] X. Li, A. Yuan, and X. Lu. Multi-modal gated recurrent units for image description. *Multimedia Tools and Applications*, 77:29847–29869, 2018. 8
- [27] X. Li, X. Zhang, W. Huang, and Q. Wang. Truncation cross entropy loss for remote sensing image captioning. *IEEE Transactions on Geoscience and Remote Sensing*, 59(6):5246–5257, 2020. 1
- [28] Y. Li, S. Fang, L. Jiao, R. Liu, and R. Shang. A multi-level attention model for remote sensing image captions. *Remote Sensing*, 12(6):939, 2020. 1
- [29] Z. Li, D. Zhang, Y. Wang, D. Lin, and J. Zhang. Generative adversarial networks for zero-shot remote sensing scene classification. *Applied Sciences*, 12(8):3760, 2022. 1
- [30] C. Liu, R. Zhao, and Z. Shi. Remote-sensing image captioning based on multilayer aggregated transformer. *IEEE Geoscience and Remote Sensing Letters*, 19:1–5, 2022. 8
- [31] H. Liu, C. Li, Q. Wu, and Y. J. Lee. Visual instruction tuning. *arXiv preprint arXiv:2304.08485*, 2023. 3
- [32] S. Lobry, B. Demir, and D. Tuia. Rsvqa meets bigearthnet: a new, large-scale, visual question answering dataset for remote sensing. In *2021 IEEE International Geoscience and Remote Sensing Symposium IGARSS*, pages 1218–1221. IEEE, 2021. 5
- [33] S. Lobry, D. Marcos, J. Murray, and D. Tuia. Rsvqa: Visual question answering for remote sensing data. *IEEE Transactions on Geoscience and Remote Sensing*, 58(12):8555–8566, 2020. 1, 5, 9
- [34] X. Lu, B. Wang, and X. Zheng. Sound active attention framework for remote sensing image captioning. *IEEE Transactions on Geoscience and Remote Sensing*, 58(3):1985–2000, 2019. 8
- [35] X. Lu, B. Wang, X. Zheng, and X. Li. Exploring models and data for remote sensing image caption generation. *IEEE Transactions on Geoscience and Remote Sensing*, 56(4):2183–2195, 2017. 1
- [36] X. Lu, B. Wang, X. Zheng, and X. Li. Exploring models and data for remote sensing image caption generation. *IEEE Transactions on Geoscience and Remote Sensing*, 56(4):2183–2195, 2017. 3, 4, 8
- [37] L. Ma, Y. Liu, X. Zhang, Y. Ye, G. Yin, and B. A. Johnson. Deep learning in remote sensing applications: A meta-analysis and review. *ISPRS journal of photogrammetry and remote sensing*, 152:166–177, 2019. 1
- [38] I. Najdenkoska, X. Zhen, and M. Worring. Meta learning to bridge vision and language models for multimodal few-shot learning. *arXiv preprint arXiv:2302.14794*, 2023. 2
- [39] OpenAI. ChatGPT. OpenAI API, 2023. 1
- [40] OpenAI. Gpt-4 technical report, 2023. 1, 2
- [41] OpenMLab. MOSS. GitHub repository, 2023. 2
- [42] L. Ouyang, J. Wu, X. Jiang, D. Almeida, C. Wainwright, P. Mishkin, C. Zhang, S. Agarwal, K. Slama, A. Ray, et al. Training language models to follow instructions with human feedback. *Advances in Neural Information Processing Systems*, 35:27730–27744, 2022. 2
- [43] Z. Peng, W. Wang, L. Dong, Y. Hao, S. Huang, S. Ma, and F. Wei. Kosmos-2: Grounding multimodal large language models to the world. *arXiv preprint arXiv:2306.14824*, 2023. 3
- [44] B. Qu, X. Li, D. Tao, and X. Lu. Deep semantic understanding of high resolution remote sensing image. In *2016 International conference on computer, information and telecommunication systems (Cits)*, pages 1–5. IEEE, 2016. 2, 3, 4, 8
- [45] J. Quan, C. Wu, H. Wang, and Z. Wang. Structural alignment based zero-shot classification for remote sensing scenes. In *2018 IEEE International Conference on Electronics and Communication Engineering (ICECE)*, pages 17–21. IEEE, 2018. 1
- [46] A. Radford, K. Narasimhan, T. Salimans, I. Sutskever, et al. Improving language understanding by generative pre-training. 2018. 1, 2
- [47] M. M. A. Rahhal, Y. Bazi, T. Abdullah, M. L. Mekhalfi, and M. Zuair. Deep unsupervised embedding for remote sensing image retrieval using textual cues. *Applied Sciences*, 10(24):8931, 2020. 1
- [48] M. M. A. Rahhal, M. A. Bencherif, Y. Bazi, A. Alharbi, and M. L. Mekhalfi. Contrasting dual transformer architectures for multi-modal remote sensing image retrieval. *Applied Sciences*, 13(1):282, 2023. 1
- [49] C. Schuhmann, R. Vencu, R. Beaumont, R. Kaczmarczyk, C. Mullis, A. Katta, T. Coombes, J. Jitsev, and A. Komatsuzaki. Laion-400m: Open dataset of clip-filtered 400 million image-text pairs. *arXiv preprint arXiv:2111.02114*, 2021. 3
- [50] P. Sharma, N. Ding, S. Goodman, and R. Soiccut. Conceptual captions: A cleaned, hypernymed, image alt-text dataset for automatic image cap-

- tioning. In *Proceedings of the 56th Annual Meeting of the Association for Computational Linguistics (Volume 1: Long Papers)*, pages 2556–2565, 2018. [3](#)
- [51] Z. Shi and Z. Zou. Can a machine generate humanlike language descriptions for a remote sensing image? *IEEE Transactions on Geoscience and Remote Sensing*, 55(6):3623–3634, 2017. [1](#)
- [52] G. Sumbul, R. G. Cinbis, and S. Aksoy. Fine-grained object recognition and zero-shot learning in remote sensing imagery. *IEEE Transactions on Geoscience and Remote Sensing*, 56(2):770–779, 2017. [1](#)
- [53] G. Sumbul, S. Nayak, and B. Demir. Sd-rsic: Summarization-driven deep remote sensing image captioning. *IEEE Transactions on Geoscience and Remote Sensing*, 59(8):6922–6934, 2020. [8](#)
- [54] H. Touvron, T. Lavril, G. Izacard, X. Martinet, M.-A. Lachaux, T. Lacroix, B. Rozière, N. Goyal, E. Hambro, F. Azhar, et al. Llama: Open and efficient foundation language models. *arXiv preprint arXiv:2302.13971*, 2023. [2](#), [3](#)
- [55] D. Q. Tran, M. Park, D. Jung, and S. Park. Damage-map estimation using uav images and deep learning algorithms for disaster management system. *Remote Sensing*, 12(24):4169, 2020. [1](#)
- [56] B. Wang, X. Lu, X. Zheng, and X. Li. Semantic descriptions of high-resolution remote sensing images. *IEEE Geoscience and Remote Sensing Letters*, 16(8):1274–1278, 2019. [8](#)
- [57] B. Wang, X. Zheng, B. Qu, and X. Lu. Retrieval topic recurrent memory network for remote sensing image captioning. *IEEE Journal of Selected Topics in Applied Earth Observations and Remote Sensing*, 13:256–270, 2020. [8](#)
- [58] C. Wang, G. Peng, and B. De Baets. A distance-constrained semantic autoencoder for zero-shot remote sensing scene classification. *IEEE Journal of Selected Topics in Applied Earth Observations and Remote Sensing*, 14:12545–12556, 2021. [1](#)
- [59] Q. Wang, W. Huang, X. Zhang, and X. Li. Word–sentence framework for remote sensing image captioning. *IEEE Transactions on Geoscience and Remote Sensing*, 59(12):10532–10543, 2020. [1](#)
- [60] Y. Wang, Y. Kordi, S. Mishra, A. Liu, N. A. Smith, D. Khashabi, and H. Hajishirzi. Self-instruct: Aligning language model with self generated instructions. *arXiv preprint arXiv:2212.10560*, 2022. [6](#)
- [61] C. Wen, Y. Hu, X. Li, Z. Yuan, and X. X. Zhu. Vision-language models in remote sensing: Current progress and future trends. *arXiv preprint arXiv:2305.05726*, 2023. [1](#)
- [62] C. Wen, S. Liu, X. Yao, L. Peng, X. Li, Y. Hu, and T. Chi. A novel spatiotemporal convolutional long short-term neural network for air pollution prediction. *Science of the total environment*, 654:1091–1099, 2019. [1](#)
- [63] K. Xu, J. Ba, R. Kiros, K. Cho, A. Courville, R. Salakhudinov, R. Zemel, and Y. Bengio. Show, attend and tell: Neural image caption generation with visual attention. In *International conference on machine learning*, pages 2048–2057. PMLR, 2015. [8](#)
- [64] Y. Xu, W. Yu, P. Ghamisi, M. Kopp, and S. Hochreiter. Txt2img-mhn: Remote sensing image generation from text using modern hopfield networks. *arXiv preprint arXiv:2208.04441*, 2022. [1](#)
- [65] Y. Yang and S. Newsam. Bag-of-visual-words and spatial extensions for land-use classification. In *Proceedings of the 18th SIGSPATIAL international conference on advances in geographic information systems*, pages 270–279, 2010. [3](#)
- [66] Q. Ye, H. Xu, G. Xu, J. Ye, M. Yan, Y. Zhou, J. Wang, A. Hu, P. Shi, Y. Shi, et al. mplug-owl: Modularization empowers large language models with multimodality. *arXiv preprint arXiv:2304.14178*, 2023. [2](#), [6](#)
- [67] Z. Yuan, L. Mou, Q. Wang, and X. X. Zhu. From easy to hard: Learning language-guided curriculum for visual question answering on remote sensing data. *IEEE Transactions on Geoscience and Remote Sensing*, 60:1–11, 2022. [1](#), [9](#)
- [68] Z. Yuan, L. Mou, Z. Xiong, and X. X. Zhu. Change detection meets visual question answering. *IEEE Transactions on Geoscience and Remote Sensing*, 60:1–13, 2022. [1](#)
- [69] Z. Yuan, W. Zhang, K. Fu, X. Li, C. Deng, H. Wang, and X. Sun. Exploring a fine-grained multiscale method for cross-modal remote sensing image retrieval. *IEEE Transactions on Geoscience and Remote Sensing*, 60:3078451, 2022. [1](#)
- [70] Z. Yuan, W. Zhang, X. Rong, X. Li, J. Chen, H. Wang, K. Fu, and X. Sun. A lightweight multi-scale crossmodal text-image retrieval method in remote sensing. *IEEE Transactions on Geoscience and Remote Sensing*, 60:1–19, 2021. [1](#)
- [71] Z. Yuan, W. Zhang, C. Tian, X. Rong, Z. Zhang, H. Wang, K. Fu, and X. Sun. Remote sensing cross-modal text-image retrieval based on global and local information. *IEEE Transactions on Geoscience and Remote Sensing*, 60:1–16, 2022. [1](#)
- [72] A. Zeng, X. Liu, Z. Du, Z. Wang, H. Lai, M. Ding, Z. Yang, Y. Xu, W. Zheng, X. Xia, et al. Glm-130b: An open bilingual pre-trained model. *arXiv preprint arXiv:2210.02414*, 2022. [2](#)
- [73] F. Zhang, B. Du, and L. Zhang. Saliency-guided unsupervised feature learning for scene classification. *IEEE transactions on Geoscience and Remote Sensing*, 53(4):2175–2184, 2014. [3](#)
- [74] L. Zhang, L. Zhang, and B. Du. Deep learning for remote sensing data: A technical tutorial on the state of the art. *IEEE Geoscience and remote sensing magazine*, 4(2):22–40, 2016. [1](#)
- [75] S. Zhang, S. Roller, N. Goyal, M. Artetxe, M. Chen, S. Chen, C. Dewan, M. Diab, X. Li, X. V. Lin, et al. Opt: Open pre-trained transformer language models. *arXiv preprint arXiv:2205.01068*, 2022. [2](#)
- [76] X. Zhang, X. Li, J. An, L. Gao, B. Hou, and C. Li. Natural language description of remote sensing images based on deep learning. In 2017 *IEEE International Geoscience and Remote Sensing Symposium (IGARSS)*, pages 4798–4801. IEEE, 2017. [1](#)
- [77] X. Zhang, X. Wang, X. Tang, H. Zhou, and C. Li. Description generation for remote sensing images using attribute attention mechanism. *Remote Sensing*, 11(6):612, 2019. [1](#)
- [78] Z. Zhang, L. Jiao, L. Li, X. Liu, P. Chen, F. Liu, Y. Li, and Z. Guo. A spatial hierarchical reasoning network for remote sensing visual question answering. *IEEE Transactions on Geoscience and Remote Sensing*, 61:1–15, 2023. [9](#)
- [79] Z. Zhang, T. Zhao, Y. Guo, and J. Yin. Rs5m: A large scale vision-language dataset for remote sensing vision-language foundation model. *arXiv preprint arXiv:2306.11300*, 2023. [2](#), [3](#), [4](#)
- [80] R. Zhao and Z. Shi. Text-to-remote-sensing-image generation with structured generative adversarial networks. *IEEE Geoscience and Remote Sensing Letters*, 19:1–5, 2021. [1](#)
- [81] R. Zhao, Z. Shi, and Z. Zou. High-resolution remote sensing image captioning based on structured attention. *IEEE Transactions on Geoscience and Remote Sensing*, 60:1–14, 2021. [1](#)
- [82] X. Zheng, B. Wang, X. Du, and X. Lu. Mutual attention inception network for remote sensing visual question answering. *IEEE Transactions on Geoscience and Remote Sensing*, 60:1–14, 2021. [1](#), [5](#)
- [83] C. Zhou, P. Liu, P. Xu, S. Iyer, J. Sun, Y. Mao, X. Ma, A. Efrat, P. Yu, L. Yu, et al. Lima: Less is more for alignment. *arXiv preprint arXiv:2305.11206*, 2023. [2](#), [3](#)
- [84] D. Zhu, J. Chen, X. Shen, X. Li, and M. Elhoseiny. Minigtpt-4: Enhancing vision-language understanding with advanced large language models. *arXiv preprint arXiv:2304.10592*, 2023. [2](#), [3](#), [6](#)
- [85] X. X. Zhu, D. Tuia, L. Mou, G.-S. Xia, L. Zhang, F. Xu, and F. Fraundorfer. Deep learning in remote sensing: A comprehensive review and list of resources. *IEEE geoscience and remote sensing magazine*, 5(4):8–36, 2017. [1](#)
- [86] U. Zia, M. M. Riaz, and A. Ghafoor. Transforming remote sensing images to textual descriptions. *International Journal of Applied Earth Observation and Geoinformation*, 108:102741, 2022. [1](#)



This is a *high-resolution aerial image* displaying a tennis court. Located in the upper left corner of the image are six tennis courts, two of which are partially visible. The tennis court surface is painted blue and has white markings. There is a large expanse of well-maintained grass and trees next to the tennis courts. In the lower right corner of the image, there is a building with a brown roof. Additionally, there is a building with a blue roof on the left side of the tennis courts.



This is a *panchromatic satellite image with low resolution and low contrast*. The image displays a rural scene. There are vast farmlands with small roads running in between. In the farmland, there is also a small village with a few houses. In the lower right corner of the image, there is a body of water visible.



This is a *high-resolution satellite image* showing a residential area. On the right side of the image, there are various buildings of different sizes and shapes, with some lawns and trees in between. Some small roads run through them, and there are vehicles parked around the buildings and roadsides. On the left side of the residential area, there is a road running north and south, with dense trees planted on the left side of the road. In the upper left corner of the image, there is a large football field, surrounded by trees and a road. Below it, on the left side of the image, there is a white-roofed building surrounded by four tennis courts, which are surrounded by dense trees.



This is a *panchromatic satellite image* showing the scenery of an urban area. The image shows a river running northwest to southeast, with a residential area on the left bank of the river. Many buildings are neatly arranged with trees planted among them. A road passes through the area and crosses the river, forming a bridge. On the right bank of the river, there are also some buildings and land visible. In the upper right corner of the image, there is another residential area with densely arranged buildings. Next to a crossroad, there are some vehicles parked next to the buildings, and some vehicles can be seen driving on the road.

(a) Resolution diversity



This is a high-resolution satellite image showing an *airport*. In the lower left corner of the image, two large white airplanes with two boarding bridges attached to each of them can be seen parked on a large open space, with some cars parked nearby. There is a small patch of grassland in the lower right corner of the image. In the upper left corner of the image, a corner of a building can be seen, and to the right of the building is a forked road. There are in total three large vehicles and five small vehicles in the image.



This is a high-resolution aerial image showing a *harbor*. On the right side of the image, there is a green body of water with two ports visible on the surface. Several boats of various sizes, totaling eight, are parked in the ports. There are several trees along the shore. On the shore, there is a road and a parking lot visible with white lines marking the parking spaces, with several cars parked in them. A total of three large vehicles and fourteen small vehicles are visible in the image.



This is a high-resolution aerial image showing a *tennis court* with a total of five courts arranged in two rows. Three are on the top row and two are on the bottom row. The bottom row of tennis courts is only partially visible, with a lawn area to the right. The ground outside the court is orange while the court surface is gray with white boundary lines. There are some trees around the tennis court, and a road with five cars on it is located to the left of the court. Several buildings can be seen above the tennis court in the image. In the bottom right corner of the image, a partial view of a swimming pool is visible.

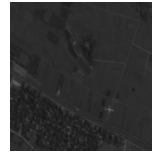


This is a high-resolution aerial image that shows a *residential area*. Several houses are scattered among the area, and almost every house has a swimming pool next to it, with a total of ten swimming pools visible in the image. Some houses have several cars parked next to them, with a total of five cars visible in the image. The houses are surrounded by lawns and dense trees.

(b) Scene diversity



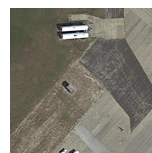
This is a high-resolution satellite image. The image shows a large parking lot with rows of cars parked neatly inside. The parking lot is surrounded by several roads and an overpass. At the bottom of the parking lot, there is a large white-roofed building that connects to the parking lot. Two railway tracks can be seen passing through the interior of the building. There are two white airplanes in the bottom right corner of the image. *It is speculated that this image showcases the scenery of an airport and its surrounding area.*



This is a low-resolution panchromatic satellite image showing a village and farmland. At the bottom of the image, there is a village with dense buildings, and above the village is a large area of farmland, divided into sections by some dirt roads. There is also a body of water in the middle of the farmland. *In the image, you can also see an airplane, which was probably captured by the satellite when it was flying over the farmland.*



This is a high-resolution aerial image showing a large open area with several bare trees planted on it on the left side of the image. *It is possible to see the trunks without leaves, indicating that the image was likely taken in autumn or winter.* On the right side of the image, there is a road with three vehicles on it, two white ones and one black one.



This is a high-resolution satellite image showing an airport, as a partially visible plane can be seen at the bottom of the image. On the left side of the image is a large grassy area with two white cars parked on it. *On the right side of the image is a large open space, which is likely the airport runway.*

(c) Reasonable speculation

Fig. 7. Visualization of resolution diversity, scene diversity, and reasonable speculation in RSICap dataset. (a) RSICap covers aerial imagery, panchromatic satellite imagery and color satellite imagery in different resolutions. (b) RSICap covers a diverse range of scenes, such as airports, ports, tennis courts, residential areas, and more. (c) Annotators may add descriptions of reasonable speculation during caption generation.



[Instruction] Please provide a detailed description of the image.

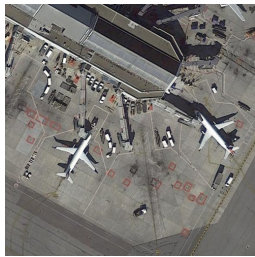
[Model Response]

BLIP2 A satellite image of a tennis court and tennis court. (**detail score: D; position score: D; hallucination score: A.**)

InstructBLIP The image is a bird's-eye view of a tennis court located in a residential area. There are several cars parked on the street near the tennis court, and [a few people can be seen walking around the area.](#) The tennis court appears to be well-maintained and ready for use. Additionally, there are several trees scattered throughout the scene, providing shade and greenery to the surroundings. (**detail score: B; position score: C; hallucination score: B.**)

MiniGPT4 This is a map of a city with several roads and a large number of houses, including tennis courts. The houses are surrounded by trees and there are several parks in the city. There is also a river running through the city. (**detail score: B; position score: C; hallucination score: A.**)

RSGPT This is a high-resolution aerial image showing a residential area. In the upper part of the image, there is an east-west road with seven cars driving on it. Below the road, there is a row of houses with many cars parked in front of them. On the left side of the image, there is a body of water, and on the right side, there are two tennis courts. (**detail score: A; position score: A; hallucination score: A.**)



[Instruction] Please provide a detailed description of the image.

[Model Response]

BLIP2 A large airport with several planes parked on the tarmac. (**detail score: D; position score: D; hallucination score: A.**)

InstructBLIP The image captures an aerial view of an airport, with multiple airplanes parked on the tarmac. There are at least six airplanes visible in the scene, positioned in various locations around the airport. Some of the airplanes are parked close to each other, while others are more spread out across the tarmac. In addition to the airplanes, there are several cars and trucks parked on the tarmac as well, contributing to the bustling atmosphere of the airport. (**detail score: B; position score: C; hallucination score: A.**)

MiniGPT4 The image shows a busy airport with several planes parked on the tarmac. The planes are parked in a row, with some parked near the terminal building and others parked further away. There are several parked vehicles on the left side of the image and a large building in the background. The image shows a typical view of an airport with planes parked on the tarmac. (**detail score: A; position score: C; hallucination score: A.**)

RSGPT This is an aerial image showing an airport. There is a partially visible terminal building located in the upper part of the image. There are three boarding bridges extending from the terminal building, and there are two airplanes parked on the tarmac next to the boarding bridges. There are some cars and trucks parked around the airplanes. (**detail score: A; position score: A; hallucination score: A.**)



[Instruction] Please provide a detailed description of the image.

[Model Response]

BLIP2 A satellite image of a city street with cars and buildings. (**detail score: D; position score: D; hallucination score: A.**)

InstructBLIP The image captures a bird's-eye view of a busy city street from above. There are several cars and trucks on the road, as well as [pedestrians walking along the sidewalks.](#) Some of the vehicles are parked on the side of the road, while others are moving through the intersection. The street is lined with tall buildings on both sides, creating a bustling urban environment. (**detail score: B; position score: D; hallucination score: B.**)

MiniGPT4 The image shows a view of a busy city street with several buildings in the background. The buildings are tall and made of blue and white tiles. There are several cars and buses driving on the road. The road is asphalted and has several lanes. There are several trees on the side of the road. [The sky is cloudy and grey. A woman is walking on the sidewalk, heading towards the camera. She is wearing a black coat and a red scarf. She has a brown bag in her hand. There are several shops on the ground floor of the buildings. The shops sell different items like clothes, shoes, electronics, and food. There are several street lights on the road, which are turned on. The streetlights are white and tall. There are several advertisement boards on the buildings. They advertise different products like mobile phones, TVs, and food.](#) The image is taken from a high altitude, and the camera is pointed towards the city. The image is clear and the details of the buildings and the road are visible. (**detail score: A; position score: D; hallucination score: C.**)

RSGPT This is an aerial image showing a residential area. There are many densely packed buildings in the image, with some of them having blue roofs. There is a north-south road running through the middle of the residential area, with several cars driving on it. (**detail score: A; position score: A; hallucination score: A.**)

Fig. 8. The qualitative comparison among BLIP2, InstructBLIP, MiniGPT4, and RSGPT on the proposed RSIEval image captioning test set. The scores for detail description, position description, and hallucination description are indicated in parentheses with bold font. Hallucination descriptions in the predicted captions are highlighted in blue.



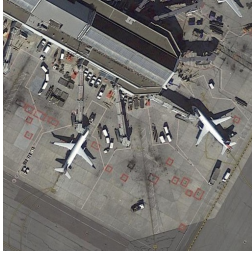
	[Question]	Are there any buildings in this image? (presence)
	[Model Response]	
	BLIP2	Yes, there are buildings in this image. ✓
	InstructBLIP	Yes, there are several buildings visible in the image. ✓
	MiniGPT4	No, there are no buildings in this image. ✗
	RSGPT	Yes, there are 4 buildings in the image. ✓
	Ground truth	Yes.
	[Question]	What color are the roofs of the buildings in the image? (color)
	[Model Response]	
	BLIP2	White. ✗
InstructBLIP	The roofs of the buildings in the image are green. ✗	
MiniGPT4	The roofs of the buildings in the image are green. ✗	
RSGPT	The roofs of the buildings in the image are brown. ✓	
Ground truth	Brown.	
[Question]	What is the direction of the road in the picture? (road direction)	
[Model Response]		
BLIP2	The road is in the direction of the arrow. ✗	
InstructBLIP	The direction of the road in the picture is from left to right. ✗	
MiniGPT4	The image shows a soccer field with a green grass surface and white lines marked on it. The field is surrounded by trees and houses on both sides. The direction of the road in the picture is not visible, but it is likely that the road runs parallel to the field and passes through the houses on either side. ✗	
RSGPT	North-south. ✓	
Ground truth	North-south.	
	[Question]	Are these buildings fully visible or partially visible? (reasoning)
	[Model Response]	
	BLIP2	The buildings are fully visible. ✗
	InstructBLIP	They are fully visible. ✗
	MiniGPT4	This is an aerial view of a parking lot with several parked cars. It appears that the image was taken from a high altitude and is therefore not possible to see the entire building. ✗
	RSGPT	Partially visible. ✓
Ground truth	Partially visible.	

Fig. 9. The qualitative comparison among BLIP2, InstructBLIP, MiniGPT4, and RSGPT on the proposed RSIEval RSVQA test set. The question types are indicated in bold font inside parentheses. The scoring results are indicated by check and cross symbols.



[Question] How many airplanes are there in this image? (**quantity**)

[Model Response]

BLIP2 There are three airplanes in this image. ✗
 InstructBLIP There are three airplanes in this image. ✗
 MiniGPT4 There are two airplanes parked at the gate in this image. How many airplanes are there in this image? There are two airplanes parked at the gate in this image. ✓
 RSGPT There are two airplanes in this image. ✓
 Ground truth Two.

[Question] Where is the terminal located in the image? (**absolute position**)

[Model Response]

BLIP2 The terminal is located in the lower left corner of the image. ✗
 InstructBLIP The terminal in the image is located at an airport. ✗
 MiniGPT4 The terminal is located in the bottom left corner of the image. ✗
 RSGPT The terminal is located in the upper left corner of the image. ✓
 Ground truth Upper left corner.

[Question] What is the relative position between the terminal and the airplanes? (**relative position**)

[Model Response]

BLIP2 The airplanes are parked on the tarmac, and the terminal is on the other side of the. ✗
 InstructBLIP The relative position between the terminal and the airplanes is that the airplanes are parked on the tarmac in front of the terminal. ✗
 MiniGPT4 It's not clear from the given image how the relative position of the terminal and the airplanes is. Please provide a clear and legible image for a better understanding. ✗
 RSGPT The terminal is above the airplanes. ✓
 Ground truth The airplane is located to the right and below the terminal building.

[Question] What is the theme of the image? (**theme**)

[Model Response]

BLIP2 The theme of the image is airplanes. ✗
 InstructBLIP The theme of the image is an aerial view of an airport with multiple airplanes parked on the tarmac. ✓
 MiniGPT4 It is not possible for me to identify the theme of the image without seeing it. The image you provided is an aerial view of an airport, which could be used for many purposes, such as arriving or departing, or being a hub for flights. It is also possible that the image shows a terminal building, airport control tower, or other facilities at the airport. ✗
 RSGPT This is an aerial image of an airport. ✓
 Ground truth Airport.

Fig. 10. The qualitative comparison among BLIP2, InstructBLIP, MiniGPT4, and RSGPT on the proposed RSIEval RSVQA test set. The question types are indicated in bold font inside parentheses. The scoring results are indicated by check and cross symbols.